Space-resolved density diagnostic of a highly ionized holmium ($Z=67$) laser-produced plasma from $3d^{10}4l$-$3d^{10}4l'$ Cu I–like lines

P. Mandelbaum and E. Behar
Racah Institute of Physics, Hebrew University, 91904 Jerusalem, Israel

J. F. Seely, U. Feldman, and C. M. Brown
E. O. Hulburt Center for Space Research, Naval Research Laboratory, Washington, D.C. 20375-5352

B. A. Hammel, C. A. Back, R. W. Lee, and D. R. Kania
Lawrence Livermore National Laboratory, University of California, Livermore, California 94550

A. Bar-Shalom
Nuclear Research Center of the Negev, P.O. Box 9001, Beer Sheva, Israel
(Received 17 December 1993)

A space-resolved electron density diagnostic of a holmium laser-produced plasma has been performed using the intensity ratios of Cu I–like $3d^{10}4l$-$3d^{10}4l'$ lines. The atomic theoretical model of the Cu I–like ion included the $3d^{10}nl$ levels with $n=4,5$ and $l=s,p,d,f$. The effect of line absorption at high electron densities is discussed and the atomic data obtained with the HULLAC computer code are compared with previously published data.

PACS number(s): 52.25.Nr, 31.20.Tz, 32.30.Rj

I. INTRODUCTION

High resolution extreme UV spectroscopy is an efficient tool for the diagnosis of laser-produced plasmas. In a recent study [1], it was shown that Cu I–like resonant lines from $3d^{10}4l$-$3d^{10}4l'$ transitions can be used as an electron density diagnostic in the 10^{18}–10^{22} cm^{-3} density range. In this previous work, a general description of the theoretical method was presented. Calculation of line intensity ratios was also given for some selected Cu I–like ions (Nd XXXII, Lu XLIII, Pb LIV, and U LXIV) using published energy levels [2] and collision and oscillator strengths [3]. Finally, the importance of the opacity effects was outlined. In the present work a similar model is used to predict electron density in a Holmium ($Z=67$) laser-produced plasma. The Holmium case is unique in that the three prominent lines $^2S_{1/2}$-$^2P_{3/2}$ ($\lambda=88.053$ Å), $^2P_{3/2}$-$^2D_{5/2}$ ($\lambda=88.350$ Å), and $^2D_{5/2}$-$^2F_{7/2}$ ($\lambda=88.655$ Å) lie in a very narrow wavelength range, and this mitigates the need for a wavelength-dependent intensity calibration of the spectrometer. Results of the theoretical model are compared with a space resolved spectrum from a laser-produced Holmium plasma.

II. EXPERIMENT

A thick Ho foil was irradiated by one beam of the Nova laser at Lawrence Livermore National Laboratory. The beam delivered 1 kJ energy in a pulse of 1 ns duration and with wavelength 0.53 μm. The focal spot had a diameter of 400 μm, and the focused intensity was 10^{15} W/cm^2. The spatially resolved XUV spectrum from the Ho plasma was recorded by a 3 m grazing incidence spectrograph that viewed the plasma at an angle of 6° to the plane of the foil. A grazing incidence mirror formed a line image of the source plasma on the entrance slit. In this way, one-dimensional spatial resolution of the source plasma was obtained along the spectral line [4,5]. The spectrum was recorded on Kodak type 101 emulsion plates, and the spectrum was scanned and digitized to obtain a 256×256 pixel image of the relevant spectral region (see Fig. 1). Each pixel corresponds to a step of 40 μm on the plate. The aperture used for the densitometer scans was 50×200 μm with the long dimension in the direction of the spectral lines. Twenty-five horizontal scans of total width 1 mm on the plate were then summed to improve the signal-to-noise ratio. Seven such scans were obtained. Since the magnification factor is 50, 1 mm on the plate corresponds to 20 μm in the target plane. A typical scan, corresponding to a region of the plasma extending from 100–120 μm from the original target surface is shown in Fig. 2.

III. THEORY

In the present work, a model of the Cu I-like Holmium ion including the 14 $3d^{10}nl$ levels ($l=s,p,d,f$ and $n=4,5$) has been developed using the HULLAC atomic physics package [6,7] of computer programs. A comparison between the results of the computations of oscillator strength and effective collision strength using the HULLAC code and the results published in Ref. [3] is given in Table I for the case of Cu I-like Neodymium. In Ref. [3], full computations were performed only for a few selected ions, the results for the other (including Holmium) ions being obtained by interpolation fit. Also, this enables us to check our collisional radiative model with the results for Nd published in Ref. [1]. Table I shows that there is

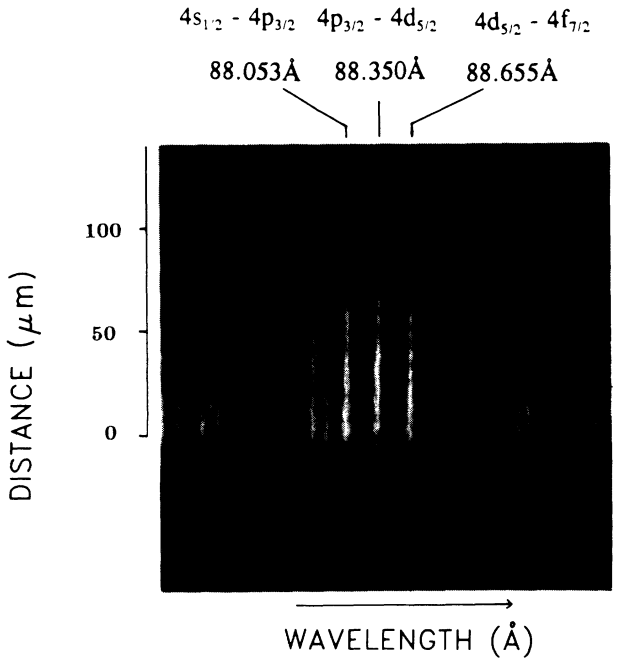

FIG. 1. The recorded experimental XUV spectrum of the Holmium laser-produced plasma (86.25 Å $<\lambda<$ 90.58 Å). The spectrum is spatially resolved in the vertical direction along the spectral lines, and this direction corresponds to the direction perpendicular to the target surface.

a very good agreement between the two sets of calculations. For the effective collision strengths the discrepancy is less than 3%. At higher electron energies HULLAC gives consistently higher collision strengths than those of Ref. [3]. The agreement between the results of our collision radiative model for Nd at $kT_e=600$ eV with those of Ref. [1] was also found to be excellent. The present calculations were performed with a version of the HULLAC code implemented on a PC-486 computer running at 33 MHz. It took about 1 h of computation time to perform the Nd computation including all the transitions between the 14 levels (from these computations, only the results for $4l$-$4l'$ transitions are displayed in Table I).

In Ref. [1], the authors predicted that opacity effects could be expected to play a significant role in line intensity ratios. At first, a collisional radiative model of Ho was performed assuming the plasma as perfectly thin at electron temperatures corresponding to one-half (890 eV), one (1780 eV), and two times (3560 eV) the ionization energy of the Cu I–like Ho ion. The results showed that the line intensity ratios are almost insensitive to these electron temperature changes. The results for $kT_e=1780$ eV are shown in Fig. 3. It shows that the lines can be used or electron density diagnostic in the 10^{18}–10^{21} cm^{-3} density range. The effect of opacity was then introduced through a simplified zero-dimensional escape-factor treatment [8,9]. This involved the correction of the Einstein coefficients appearing in the rate equations in the following manner:

$$A_{ij}\rightarrow\epsilon_{ij}A_{ij}\ , \tag{1}$$

where

$$e_{ij}=(1/\tau_{ij}\sqrt{\pi})\int_{-\infty}^{+\infty}\{1-\exp[-\tau_{ij}\exp(-y^2)]\}dy \tag{2}$$

is the "escape factor" and

$$\tau_{ij}=\frac{\pi e^2}{mc\sqrt{\pi}}\frac{2\sqrt{\ln 2}}{\Delta_D}f_{ij}n_iL \tag{3}$$

is the optical depth at line center for the transition $j\rightarrow i$. $\Delta_D(T_I)$ is the Doppler width at ion temperature T_I, f_{ij} is the oscillator strength of the transition, n_i is the population density of the absorbing state, and L is the width of the plasma column. The coupled quantities n_i and ϵ_{ij} are determined by solving iteratively the steady-state collisional-radiative rate equations until convergence is attained in the level populations. The following condi-

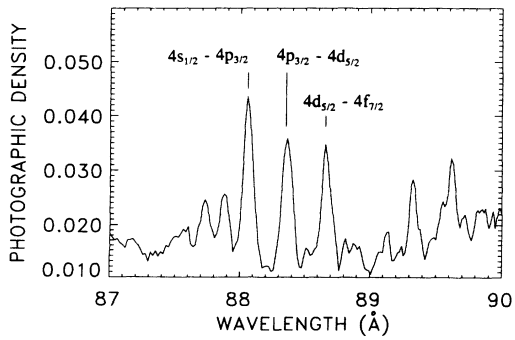

FIG. 2. Typical scan of the experimental spectrum corresponding to a region extending from 100 to 120 μm from the target surface. The three lines used for density diagnostic are indicated.

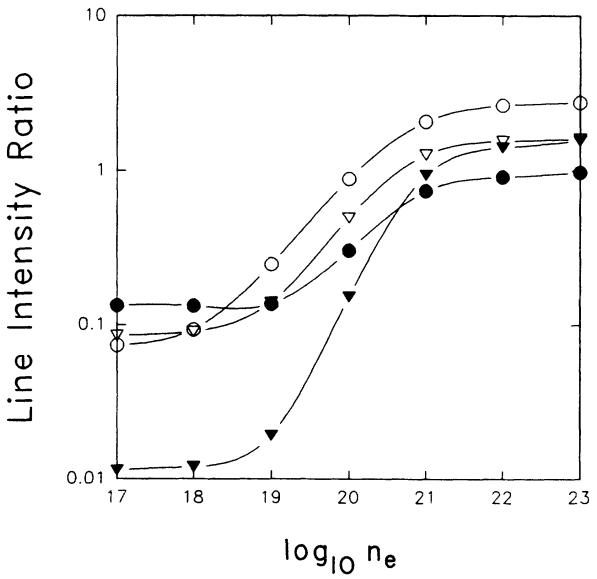

FIG. 3. Density-sensitive line ratio for Ho XXXIX (assuming thin plasma) at $kT_e=1780$ eV: ▽ $I(^2P_{3/2}$-$^2D_{5/2}$ (λ=88.350 Å))/$I(^2S_{1/2}$-$^2P_{3/2}$ (λ=88.053 Å)); ▼ $I(^2D_{5/2}$-$^2F_{7/2}$ (λ=88.655 Å))/$I(^2S_{1/2}$-$^2P_{3/2}$ (λ=88.053 Å)); ○ $I(^2P_{1/2}$-$^2D_{3/2}$ (λ=66.145 Å))/$I(^2S_{1/2}$-$^2P_{3/2}$ (λ=88.053 Å)), ● $I(^2D_{5/2}$-$^2F_{7/2}$ (λ=88.655 Å))/$I(^2P_{3/2}$-$^2D_{5/2}$ (λ=88.350 Å)).

tions were assumed: $T_I = 1/2T_e$, the Cu I–like fraction $n_{\text{Cu I-like}} = 0.10$, and an average degree of ionization $Z_{\text{av}} = 38$. The size of the plasma was taken as 200 μm, which was approximately equal to the laser focal spot radius. The results of the calculation including the opacity effect are given in Fig. 4. The two relevant line intensity ratios are $R_1 = I(^2P_{3/2}\text{-}^2D_{5/2}$ ($\lambda = 88.350$ Å$))/I(^2S_{1/2}\text{-}^2P_{3/2}$ ($\lambda = 88.053$ Å)) (∇ in Figs. 3 and 4), and $R_2 = I(^2D_{5/2}\text{-}^2F_{7/2}$ ($\lambda = 88.655$ Å$))/I(^2S_{1/2}\text{-}^2P_{3/2}$ ($\lambda = 88.053$ Å)) ▼ in Figs. 3 and 4).

For $N_e < 10^{19}$ cm^{-3}, the two models give the same results for the line intensity ratios. At higher densities the results are slightly different. The model including the opacity effect predicts that, at $n_e = 10^{21}$ cm^{-3}, $R_1 = R_2 = 1$ and this value remains constant at higher densities. This is in contradistinction with the thin plasma model where R_1 and R_2 reach their final value (about 1.5) at $n_e = 10^{22}$ cm^{-3}. In the intermediate electron density range, 10^{19} cm$^{-3} < n_e < 10^{21}$ cm^{-3}, R_1 and R_2 are useful as electron density diagnostics but opacity effects can introduce an error in the electron density estimation of about 30% if opacity effects were not considered.

IV. COMPARISON WITH EXPERIMENT

For the seven scans derived from the digitized spectrum, the line ratios were obtained as a function of the

TABLE I. Comparison of the computed f values and collision strength in Cu I–like Nd XXXII for (1) the results of Zhang, Sampson, and Fontes (Ref. [3]) and (2) the present work using the HULLAC code. The numbers in brackets denote multiplicative powers of ten.

			$\Omega(E')$					
Transition	Source	f	$E'=0.001$	$E'=0.005$	$E'=0.015$	$E'=0.04$	$E'=0.09$	$E'=0.18$
$4s\text{-}4p_{1/2}$	(1)	0.1505	8.09[−1]	8.38[−1]	9.01[−1]	1.04	1.19	1.38
	(2)	0.1515	8.12[−1]	8.43[−1]	9.10[−1]	1.04	1.21	1.39
$4s\text{-}4p_{3/2}$	(1)	0.4644	1.42	1.47	1.59	1.80	2.11	2.43
	(2)	0.4670	1.43	1.48	1.60	1.82	2.14	2.46
$4s\text{-}4d_{3/2}$	(1)		9.18[−2]	9.37[−2]	9.75[−2]	1.03[−1]	1.09[−1]	1.13[−1]
	(2)		9.33[−2]	9.50[−2]	9.87[−2]	1.05[−1]	1.11[−1]	1.16[−1]
$4s\text{-}4d_{5/2}$	(1)		1.37[−1]	1.40[−1]	1.46[−1]	1.55[−1]	1.64[−1]	1.70[−1]
	(2)		1.39[−1]	1.42[−1]	1.47[−1]	1.57[−1]	1.67[−1]	1.74[−1]
$4s\text{-}4f_{5/2}$	(1)		2.20[−2]	2.19[−2]	2.16[−2]	2.14[−2]	2.14[−2]	2.20[−2]
	(2)		2.19[−2]	2.18[−2]	2.16[−2]	2.15[−2]	2.19[−2]	2.29[−2]
$4s\text{-}4f_{7/2}$	(1)		2.91[−2]	2.90[−2]	2.88[−2]	2.86[−2]	2.87[−2]	2.96[−2]
	(2)		2.93[−2]	2.92[−2]	2.90[−2]	2.88[−2]	2.94[−2]	3.08[−2]
$4p_{1/2}\text{-}4p_{3/2}$	(1)		1.40[−1]	1.38[−1]	1.34[−1]	1.29[−1]	1.24[−1]	1.22[−1]
	(2)		1.40[−1]	1.38[−1]	1.35[−1]	1.29[−1]	1.25[−1]	1.24[−1]
$4p_{1/2}\text{-}4d_{3/2}$	(1)	0.6336	1.19	1.23	1.32	1.51	1.76	2.07
	(2)	0.6350	1.20	1.24	1.33	1.52	1.78	2.08
$4p_{1/2}\text{-}4d_{5/2}$	(1)		2.59[−2]	2.54[−2]	2.47[−2]	2.42[−2]	2.45[−2]	2.57[−2]
	(2)		2.60[−2]	2.56[−2]	2.49[−2]	2.44[−2]	2.50[−2]	2.67[−2]
$4p_{1/2}\text{-}4f_{5/2}$	(1)		1.03[−1]	1.05[−1]	1.11[−1]	1.20[−1]	1.29[−1]	1.37[−1]
	(2)		1.05[−1]	1.08[−1]	1.13[−1]	1.23[−1]	1.33[−1]	1.41[−1]
$4p_{1/2}\text{-}4f_{7/2}$	(1)		1.28[−2]	1.23[−2]	1.14[−2]	1.01[−2]	9.49[−3]	9.63[−3]
	(2)		1.33[−2]	1.27[−2]	1.15[−2]	1.02[−2]	9.63[−3]	9.96[−3]
$4p_{3/2}\text{-}4d_{3/2}$	(1)	0.0494	3.03[−1]	3.11[−1]	3.32[−1]	3.74[−1]	4.35[−1]	4.98[−1]
	(2)	0.0495	3.04[−1]	3.14[−1]	3.35[−1]	3.78[−1]	4.41[−1]	5.06[−1]
$4p_{3/2}\text{-}4d_{5/2}$	(1)	0.4790	2.43	2.52	2.70	3.08	3.61	3.17
	(2)	0.4800	2.44	2.53	2.72	3.10	3.63	4.22
$4p_{3/2}\text{-}4f_{5/2}$	(1)		4.75[−2]	4.76[−2]	4.78[−2]	4.86[−2]	5.01[−2]	5.20[−2]
	(2)		4.84[−2]	4.83[−2]	4.83[−2]	4.92[−2]	5.12[−2]	5.37[−2]
$4p_{3/2}\text{-}4f_{7/2}$	(1)		1.94[−1]	1.98[−1]	2.06[−1]	2.21[−1]	2.34[−1]	2.45[−1]
	(2)		1.96[−1]	2.01[−1]	2.09[−1]	2.24[−1]	2.41[−1]	2.53[−1]
$4d_{3/2}\text{-}4d_{5/2}$	(1)		9.55[−2]	9.13[−2]	8.41[−2]	7.57[−2]	7.00[−2]	6.80[−2]
	(2)		9.63[−2]	9.20[−2]	8.45[−2]	7.57[−2]	7.08[−2]	6.98[−2]
$4d_{3/2}\text{-}4f_{5/2}$	(1)	0.4125	1.91	1.98	2.14	2.44	2.85	3.30
	(2)	0.4150	1.94	2.00	2.16	2.46	2.90	3.35
$4d_{3/2}\text{-}4f_{7/2}$	(1)		3.17[−2]	2.91[−2]	2.46[−2]	1.90[−2]	1.59[−2]	1.55[−2]
	(2)		3.16[−2]	2.91[−2]	2.47[−2]	1.92[−2]	1.63[−2]	1.61[−2]
$4d_{5/2}\text{-}4f_{5/2}$	(1)	0.0185	1.74[−1]	1.76[−1]	1.82[−1]	1.97[−1]	2.25[−1]	2.56[−1]
	(2)	0.0183	1.75[−1]	1.77[−1]	1.84[−1]	2.00[−1]	2.27[−1]	2.61[−1]
$4d_{5/2}\text{-}4f_{7/2}$	(1)	0.3766	2.81	2.91	3.12	3.56	4.17	4.81
	(2)	0.3783	2.84	2.94	3.16	3.60	4.21	4.90
$4f_{5/2}\text{-}4f_{7/2}$	(1)		1.27[−1]	1.13[−1]	8.92[−2]	6.25[−2]	4.72[−2]	4.20[−2]
	(2)		1.24[−1]	1.11[−1]	8.91[−2]	6.37[−2]	4.87[−2]	4.33[−2]

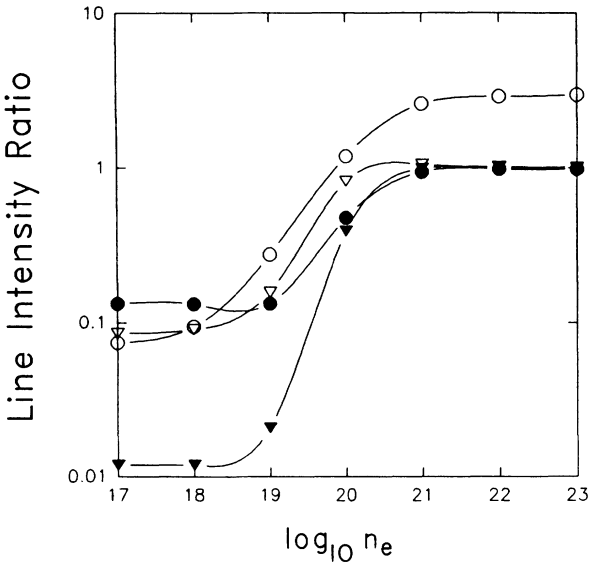

FIG. 4. Same as Fig. 3 but including the opacity effects in the model.

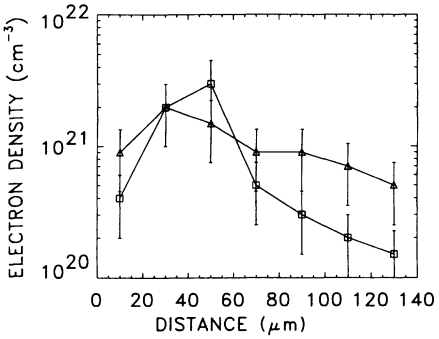

FIG. 5. Electron density as a function of the distance from the target. The electron density has been deduced from the comparison of the experimental line ratios and the results of the thick plasma model (Fig. 4) for two line ratios. □ $I(^2P_{3/2}$-$^2D_{5/2}$ (λ=88.350 Å))/$I(^2S_{1/2}$-$^2P_{3/2}$ (λ=88.053 Å)); △ $I(^2D_{5/2}$-$^2F_{7/2}$ (λ=88.655 Å))/$I(^2S_{1/2}$-$^2S_{1/2}$-$^2P_{3/2}$ (λ=88.053 Å)).

distance from the plane target in steps of 20 μm. The deduced electron densities obtained by comparing the experimental line ratios to the results of the *thick plasma model* are shown in Fig. 5.

For a distance from the target surface of $d > 50$ μm, the two line ratios give a smoothly decreasing electron density from 10^{21} cm^{-3} at $d \approx 60$ μm to $[3.5 \pm 1.5] \times 10^{20}$ cm^{-3} at $d \approx 130$ μm. The quite important discrepancy between the results of the two different line ratios can be attributed to the simplicity of the steady-state collisional-radiative model which does not take into account the effects of the expansion of the laser-produced plasma. In addition, the line ratios were derived from time-integrated photographic spectra.

From d from 0 to 50 μm, the plasma model gives an increasing of the electron density. This result is inconsistent with numerous studies that show that the electron density is higher near the target than in the corona. This inconsistency can be explained by an inadequate treatment of opacity effects. Indeed, for these spectra emitted from a region of the plasma so close to the target, electron densities are much higher and the opacity effects are very important. In addition, for $n_e > 10^{21}$ cm^{-3}, the line ratios are insensitive to electron density, and the only conclusion that can be drawn is that in the core plasma absorption effects are important and $n_e > 10^{21}$ cm^{-3}.

V. CONCLUSION

In the present study, ratios of spectral line intensities as proposed by Feldman, Doschek, and Seely [1] have been used to determine the electron density from a space-resolved spectrum of a highly ionized Holmium laser-produced plasma. The lines involved are resonant lines of the Cu I–like ions, and it is shown that these lines are useful for density diagnostics of the low electron density corona plasma. Opacity effects, which are predicted by a model including in a simple way the absorption process, are clearly observed in the spectra emitted from the higher density core plasma. The Holmium line ratios are useful as an electron density diagnostic for the range 10^{18}–10^{21} cm^{-3}. This range of electron density can be extended to higher or lower density by using Cu I–like ions with higher or lower atomic numbers than 67.

[1] U. Feldman, G. A. Doschek, and J. F. Seely, J. Appl. Phys. **68**, 3947 (1990).
[2] J. F. Seely, C. M. Brown, and U. Feldman, At. Data Nucl. Data Tables **43**, 145 (1989).
[3] H. L. Zhang, D. H. Sampson, and C. J. Fontes, At. Data Nucl. Data Tables **44**, 288 (1990).
[4] W. E. Behring, J. H. Underwood, C. M. Brown, U. Feldman, J. F. Seely, F. J. Marshall, and M. C. Richardson, Appl. Opt. **27**, 2762 (1988).
[5] W. E. Behring, R. J. Ugiansky, and U. Feldman, Appl. Opt. **12**, 528 (1973).
[6] M. Klapisch, J. L. Schwob, B. S. Fraenkel, and J. Oreg, J. Opt. Soc. Am. **67**, 148 (1977).
[7] A. Bar-Shalom, M. Klapisch, and J. Oreg, Phys. Rev. A **38**, 1773 (1988).
[8] J. L. Schwob and C. Breton, C. R. Acad. Sc. Paris **261**, 1476 (1965).
[9] W. H. Goldstein, J. Oreg, A. Zigler, A. Bar-Shalom, and M. Klapisch, Phys. Rev. A **38**, 1797 (1988).

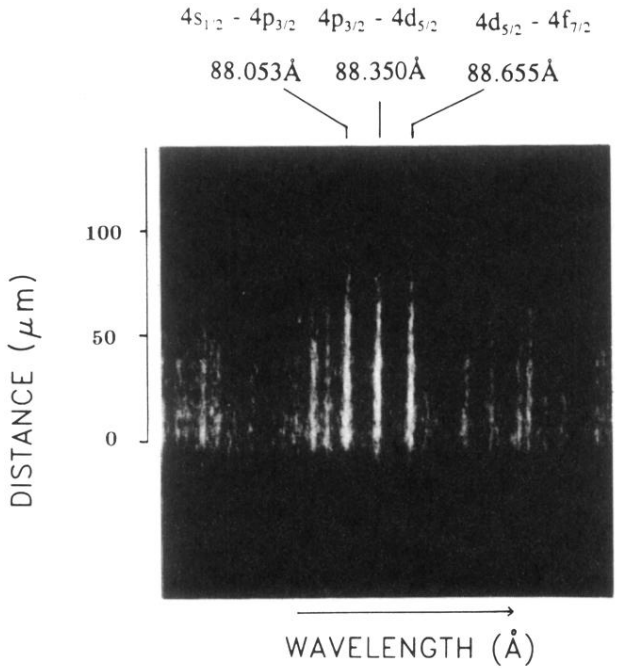

FIG. 1. The recorded experimental XUV spectrum of the Holmium laser-produced plasma (86.25 Å $< \lambda <$ 90.58 Å). The spectrum is spatially resolved in the vertical direction along the spectral lines, and this direction corresponds to the direction perpendicular to the target surface.